Australian Meteorological and Oceanographic Journal 62 (2012) 307–324

Case studies of orographic precipitation in the Brindabella Ranges: model evaluation and prospects for cloud seeding

Thomas H. Chubb, Anthony E. Morrison, Simon Caine, Steven T. Siems and Michael J. Manton
The School of Mathematical Sciences
Monash University

(Manuscript received October 2011; revised September 2012)

Recent confirmatory results in cloud seeding trials in the Australian Snowy Mountains have generated interest in performing similar experiments elsewhere. The Brindabella Ranges, which form the western border and catchment watershed of the Australian Capital Territory, share similarities in both climate and topography to the Snowy Mountains, so there is some prospect of conducting cloud seeding operations there. This paper presents an analysis of observations and high-resolution weather research and forecasting (WRF) model simulations of two wintertime storms from 2008 with the purpose of (1) evaluating the performance of the WRF model in simulating wintertime storms in the Australian alpine environment, and (2) investigating the nature of these storms from the perspective of cloud seeding research.

The WRF model results compare favourably with much of the meteorological data used. There was a tendency to simulate too much moisture in the lower levels, and as a result the simulated low-level cloud coverage was somewhat more extensive than observed. Precipitation amounts were generally well represented, but the paucity of the observational network in the Brindabella Ranges made a comprehensive evaluation impossible. Cloud liquid water path (LWP), observed with a mountain top dual-channel microwave radiometer, was surprisingly well represented by the WRF model, especially in the post-frontal conditions.

Radar reflectivity in the analysis region showed significant differences upwind and downwind of the Brindabella Ranges, suggesting that the mountains played an important role in the modulation of precipitation structures. Both of the case study storms were characterised by extended periods with appreciable quantities of supercooled liquid water, which is central to the glaciogenic cloud seeding hypothesis. However, further research would need to be conducted to determine whether such conditions occur frequently enough to permit cloud seeding operations, and whether it would be feasible to target the catchment regions with seeding material.

Introduction

Understanding of wintertime precipitation in mountainous regions is central to water resources management in the Murray-Darling Basin. The Great Dividing Range (GDR), which runs along the entire eastern seaboard of the Australian continent, forms the headwaters of all of the major rivers in this agricultural 'breadbasket'. Annual precipitation amounts are up to four times greater in these uplifted regions compared with the lower lying plains to the west (Chubb et al. 2011), and the majority of this precipitation occurs in the cooler months of May–September. A decline of about 15 per cent in cool season precipitation in southern Australia since 1958 has been observed (Nicholls 2010), and links with sea-level pressure changes have been established (Larsen and Nicholls 2009), but the impact on alpine precipitation in this region has not been specifically investigated.

Research into the meteorology of mountainous regions has failed to reach the level of interest in Australia that it has

Corresponding author address: address?

attained in other regions, owing principally to the modest topography of the continent. A climatology of wintertime precipitation in the Snowy Mountains is given by Chubb et al. (2011) for the two decades 1990–2009. This period was characterised by one of the most severe droughts in the past century during this period, with a decline in wintertime precipitation of 43 per cent detected in the high elevation ($h > 1000$ m) regions. Chubb et al. (2011) found that about 59 per cent of precipitation events, accounting for nearly 80 per cent of wintertime precipitation in the Snowy Mountains, was associated with a frontal passage. A similar climatology for the Victorian Alps was performed by Landvogt et al. (2008), who partitioned daily precipitation into a number of categories including 'pre-frontal', accounting for about half of wintertime precipitation, as well as 'post-frontal' and 'cutoff', accounting for a further 25 per cent each.

There has also been somewhat of a resurgence of interest in cloud seeding research during the recent severe droughts. A cloud seeding trial in the Snowy Mountains (Manton and Warren 2011) was begun in 2005, where the release of silver iodide from ground-based generators during wintertime (May–September) storms was shown to augment precipitation by 14 per cent (at the three per cent significance level), after accounting for the targeting of the analysis region. Conditions suitable for cloud seeding were identified when cloud top temperatures were colder than –7 °C with at least 400 m of cloud above the –5 °C level, and appreciable supercooled liquid water was available (see Manton et al. 2011 for details of additional criteria). The Brindabella Ranges, located to the west of Canberra and just to the north of the Snowy Mountains, has a comparable climate and topography, making it a potential candidate for further cloud seeding trials. These mountains are an attractive location for cloud seeding operations because of the potential to augment Canberra's catchment inflows.

The hypothesis of glaciogenic cloud seeding is that the efficiency of precipitation may be enhanced by the introduction of ice nuclei into clouds with an abundance of supercooled liquid water (Ryan and King 1997). This process should be most effective when natural ice nuclei are rare and ice processes are suppressed as a result. Moist flow over topographic barriers provides the most likely environment for these conditions (WMO 2001). A preliminary study in the Snowy Mountains region (Warburton and Wetzel 1992) used coordinated microwave radiometer and Ka-band radar observations to establish the build-up of supercooled liquid water during certain storm periods, while the abundance of ice crystals in other periods resulted in the depletion of liquid water.

The prediction of conditions during wintertime storms is an important factor in planning cloud seeding operations. The importance of orographic forcing, and the complexity of the topography in alpine environments, generally necessitates high spatial resolution in meteorological forecasts. Routine forecasts for the Brindabella region are provided by the Bureau of Meteorology using the Australian Community Climate and Earth System Simulator (ACCESS), with a grid spacing of 5 km in the highest resolution nests (NMOC 2010), which is insufficient to fully resolve the orographic impacts of the Brindabella Ranges on the local meteorology. Furthermore, evaluation of ACCESS forecasts for this locality are complicated by the sparse nature of surface observations.

Rapid improvements in both observational capabilities and computational capacity have revolutionised the meteorologist's ability to describe weather phenomena in the context of a case study analysis. Morrison et al. (2009) used satellite-born Moderate Resolution Imaging Spectroradiometer (MODIS) observations and the WRF model to investigate the prevalence of supercooled liquid and mixed-phase clouds over Tasmania and the ocean to the west (frequently upwind of the study area considered in this paper), finding that the model was generally capable of satisfactorily reproducing the statistics of cloud top microphysical properties retrieved by MODIS. Of particular relevance to this study is the recent work of Lulin et al. (in press 2012), who have implemented a full treatment of the glaciogenic cloud seeding process in the WRF model and are testing it for case studies in the southern Idaho.

In this paper, we present an analysis of two typical wintertime storms over the Brindabella Ranges to the west of Canberra and just to the north of the Snowy Mountains. The primary objective of this study is to evaluate the performance of the weather research and forecast (WRF) model run at high-resolution in simulating conditions in this region during wintertime storms. The secondary objective is to illustrate the role of orography in the life cycle of clouds and precipitation in this alpine environment, as an initial step in determining whether the Brindabella Ranges could be a suitable region to perform cloud seeding research or operations.

Analysis region, data and methods

The Brindabella Ranges and catchment area

The Brindabella Ranges are an offshoot of the GDR, and lie some 30 km to the west of Canberra, forming the northern end of the Australian Alps (Fig. 1). The mountain range forms the western border of the Australian Capital Territory, and the catchment areas along the Cotter River valley just to the east supply about 85 per cent of Canberra's water. The highest point of this range is Mt. Bimberi, reaching 1912 m above sea level, and the ranges are somewhat less elevated than the Snowy Mountains to the southwest. Nevertheless, the terrain in the region is interesting for the study of orographic precipitation, as a substantial section of the main range is oriented north–south and is raised above the surrounding area (Fig. 2).

Meteorological data sources

Measuring precipitation in an alpine region is highly challenging given its sensitivity to the local orography. This challenge is even greater during the winter when

the precipitation falls as snow or ice, and when winds are frequently strong. Additionally, access difficulties in remote locations mean that precipitation gauges networks tend to be too sparse to adequately represent the spatial patterns in precipitation. A Bureau of Meteorology automatic weather station (AWS) is located atop Mt. Ginini (148.77°E, 35.53°S; elevation 1760 m), and is equipped with a Rimco 8020 heated tipping bucket precipitation gauge, providing measurements of both frozen and liquid precipitation. The gauge is unfenced but is partially protected in a clearing formed by small trees and a shed. Data from an independent, unheated gauge network operated in the ranges by ActewAGL were also available, but it was found that the under-reporting of frozen precipitation was too severe for use in this analysis. To characterise broader-scale development of precipitation during the case study events, AWS data from Wagga Wagga AMO (125 km to the west), and Isabella Plains AWS (31 km to the east in suburban Canberra), and daily precipitation data from a large number of regional gauges are also presented

The closest regular upper-air soundings are made twice daily from Wagga Wagga, some 125 km west of Mt. Ginini. These data are presented below to show the atmospheric profile during the case study events, and to evaluate the timing of the WRF numerical model results and identify any lead or lag in the simulations.

For the winter of 2008, a dual channel microwave radiometer (Westwater 1978) providing one-minute column integrated liquid water and water vapour measurements was intermittently operated by ActewAGL at a site co-located with the Mt. Ginini AWS. Radar observations are generally available from Wagga Wagga (120 km to the west) or from Captains Flat (70 km to the east), but for the case study periods only data from the Captains Flat radar was available. The MODIS instrument is located on two of the NASA Earth Observing System satellites in sun-synchronous orbit, and passes over the Brindabella region about four times per day. The MODIS Level-2 Cloud Product (Platnick et al. 2003) includes cloud top characteristics such as temperature and phase, and a total cloud water path variable derived from visible and infrared radiances. To compare with the microwave radiometer column-integrated liquid water path, statistics of values in a small domain (0.25 × 0.25°) centred on Mt. Ginini are presented in this analysis.

Numerical simulation of case studies with the WRF model

Numerical meteorological model output, carefully interpreted, can give a richer understanding of physical processes that may not be directly observed. In particular, observations of cloud structure are limited during these two case study periods. The microwave radiometer gives high-frequency point values for column-integrated liquid water, whereas the MODIS instrument provides spatially dense observations of this parameter very infrequently. One of the motivations of this modelling study is to reconcile the observational paucity of cloud variables with simulated data.

The model was forced by boundary and initial conditions

Fig. 1. Map of southeastern Australia showing topography of the GDR. The rectangle indicates the location of the Brindabella Ranges analysis region (see Fig. 2). The two innermost model domain boundaries (at 1.35 and 4.05 km grid spacing) are shown with dashed lines. The Captains Flat radar site and the three AWS locations discussed in text are indicated by the black markers.

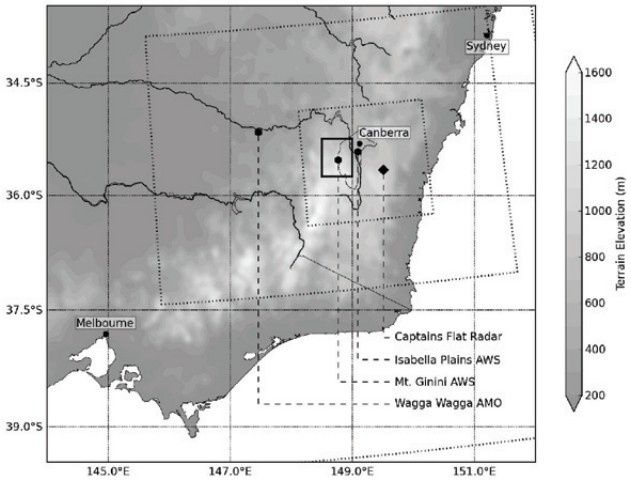

Fig. 2. Map of Brindabella region (expanded section from Fig. 1), from gridded topography used to force the numerical simulations. The Australian Capital Territory border is shown by the solid line, and the analysis region is shown by the square. Other features include waterways (thin black lines), the Snowy Mountains Highway (dashed), Bimberi Peak (triangle marker), and the Canberra reservoirs.

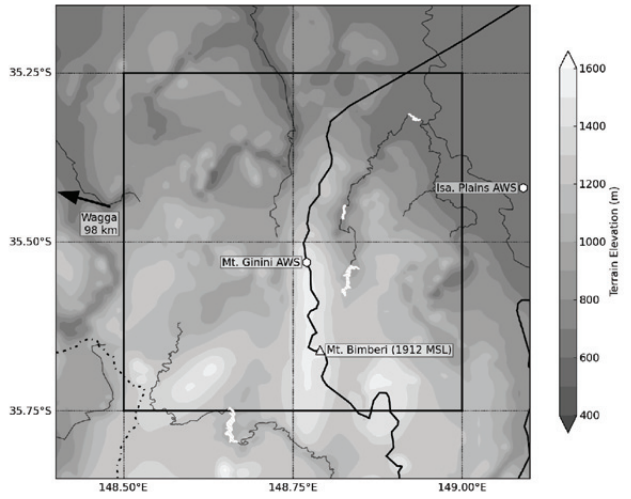

derived from the global forecast system operational analysis, which were obtained on a 1 × 1° grid, and processed with the standard WRF preprocessing system (WPS). Numerical simulations of the meteorology for the case study were performed using the non-hydrostatic advanced research WRF (ARW) version 2.2.1 (Skamarock et al. 2007). The model configuration was of five telescoping domains, each increasing the resolution by a factor of three. Feedback between the domains was switched off so that valid comparisons between

the different resolution domains could be made. The outermost domain had a grid spacing of about 110 km to match the resolution of the initial condition data covering the Australian continent and a large portion of the Southern Ocean north of 50°S, so as to directly simulate the large-scale synoptic features driving the weather in the Brindabella Ranges. The innermost nest was centred on the GDR, slightly to the east of Canberra, and had a grid spacing of 1.35 km, with a model time step of three seconds. There were 64 vertical levels, using a hybrid terrain-following/hydrostatic-pressure η coordinate. The vertical spacing increased exponentially with height with ten levels in the first 400 m, 12 levels in the next 1000 m, to a model top of about 19 000 m.

The physics options selected for these simulations are typical choices for mid-latitude meteorology in complex topography. Notably, the planetary boundary-layer scheme used was the Mellor-Yamada-Janjić scheme (Mellor and Yamada 1982), and the cloud microphysics scheme used was the Thompson microphysics (Thompson et al. 2004). The Betts-Miller-Janjić (Janjić 1994) cumulus parameterisation scheme was used in the three coarse domains to represent sub-grid scale cloud processes, but switched off for the two inner domains (at grid spacings of 4.05 and 1.35 km) as these processes were assumed to be explicitly resolved.

The choice of microphysics scheme probably has the largest impact on simulations of precipitation in complex terrain during wintertime storms such as the two case studies selected. The Thompson scheme has been developed specifically to perform well in these conditions (Stoelinga et al. 2003). It is a bulk microphysics scheme in that it does not directly predict distributions of hydrometeor size. It is double moment for cloud ice, predicting both mass and number concentrations for these hydrometeors, and single moment for cloud water, rain, snow and graupel, predicting only mass concentration. To represent aerosol loading of the atmosphere, the user specifies a cloud condensation nuclei concentration at compile time. The value selected for this parameter was 150 cm^{-3} reflective of the generally cleaner nature of the southern hemisphere air mass (Boers and Krummel 1998) .

The simulations were initialised at 1200 UTC on the first day of each of the case studies, leaving a spin-up period of at least six-hours before the first precipitation observations. They were run for a total of 60-hours, although only the first 48-hours of simulation are presented here. The evaluation performed from the model output included:

- Simulated soundings for comparison with Wagga Wagga upper air data;
- Diagnosis of cloud top temperature;
- Simulated surface precipitation in the Brindabella region at the model grid points closest to the physical locations of the gauges;
- Diagnosis of total column liquid water and water vapour at the grid point nearest Mt. Ginini for comparison with microwave radiometer observations, as well as with MODIS cloud water observations.

Synoptic meteorology and dynamics of the case study storms

The July case study was characterised by the strong dynamics of a mature extratropical cyclone. Figure 3 shows the MSLP-IR composite shortly before the frontal passage of the July storm in the Brindabella Ranges. The pattern is typical of a well-developed extratropical cyclone, with a deep frontal band extending equatorward to the subtropics followed by a 'dry slot' in the subsiding region behind the front. A high cloud streak above the frontal band demarcates the location of the jet stream maximum. Not analysed in these charts, but certainly present in geostationary satellite water vapour retrievals (not shown), is an occlusion forming to the southwest of the system over the southern coastline of the continent. Large-scale convective cloud exists near the surface low pressure centre.

The August storm, depicted in Fig. 4 just after the frontal passage in the Brindabella Ranges, is of quite a different nature. The surface depression is much shallower and less organised than for the July storm, and in this case the system is isolated from the subtropics by a strong ridge on the equatorward side. Cold air advection is apparent from the cumulus field on the western side of the system.

To enhance the structure of the analysis, two 12-hour intervals were identified for each of the case study periods. For the July case, these were from 0000–1200 UTC 20 July and 1500–0300 UTC 20–21 July; for the August case the intervals were 1800–0600 UTC 09–10 August and 0700–1900 UTC 10 August). These intervals were subjectively chosen to capture the main frontal passage characterised by heavy precipitation, and the subsequent post-frontal period characterised by light precipitation and persistent cloud, and each of the analyses presented in the following sections correspond to these intervals.

Figures 5 and 6 show observed soundings from Wagga Wagga and the simulated atmospheric profile at the nearest grid point in the 4.05 km domain. Small differences in the timing due to the forcing by the boundary conditions may be identified in this manner; for example in the July case the best matching simulated profile leads the observation by an hour at 0000 UTC 21 July. These timing differences were also apparent when comparing the surface observations and cloud top features with model-derived parameters.

The sounding at 0000 UTC 20 July (Fig. 5(a)) roughly coincided with the frontal passage at Wagga Wagga. Deep moisture is apparent in the sounding between 700 and 400 hPa, with an 'inverted-V' profile below cloud base indicating a deep, well-mixed boundary layer. The WRF simulation captures these features, but the simulated profile is substantially moister at lower levels, suggesting a cloud base as low as 800 hPa. The strong inversion below 850 hPa is not a feature of the cool change, as the low-level winds are clearly from the north. The change is apparent in the simulated profile one hour later (not shown), with a wind direction shift of about 120°. The strength of the change associated

Fig. 3. Mean sea-level pressure (MSLP) manual analyses, overlaid on MTSAT-1R infrared imagery, for July case (0000 UTC 20 July 2008). Copyright of Australian Bureau of Meteorology.

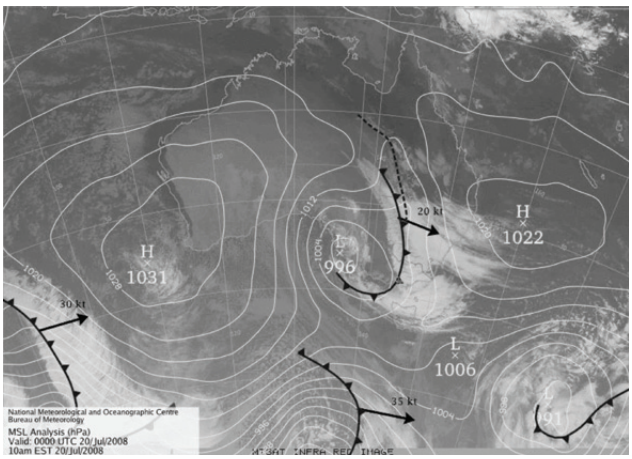

Fig. 4. As for Fig. 3, but for August case (0000 UTC 10 August 2008). Copyright of the Australian Bureau of Meteorology.

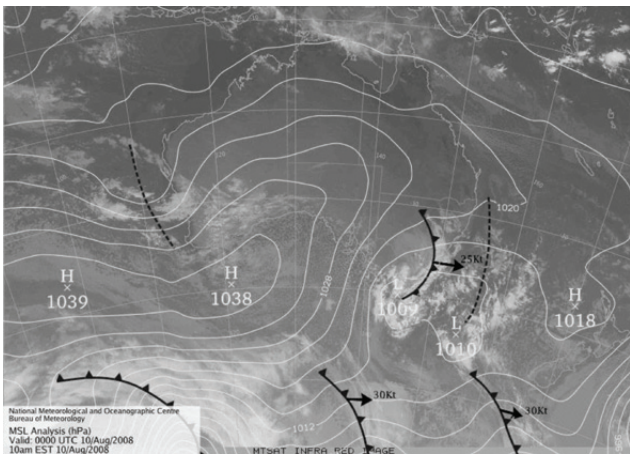

with this system is apparent in the differences between the pre- and post-frontal profiles, with the sounding at 0000 UTC 21 July being about 5 °C cooler at the 500 hPa level and a distinct drop of the tropopause from about 225 hPa to 360 hPa.

No sounding immediately prior to the frontal passage for the August case was available, so only the simulated profile at 1800 UTC 09 August is shown in Fig. 6(a). An 'inverted- V' profile below 800 hPa with a strong low-level inversion was once again present, but the winds are weaker and the pre-frontal air mass is substantially cooler than for the July case. The directional change in the wind following the frontal passage (Fig. 6(b)) was quite small, and above 800 hPa there was little change in the temperature or moisture profile. The simulated post-frontal profile is cooler, moister and more stably stratified than the sounding below 850 hPa, but both the model and the sounding indicate a stable layer around 700 hPa with drier air above this level.

MODIS and WRF cloud top retrievals

Cloud top temperature is provided by NASA as a level two product derived using the CO2 slicing technique Menzel et al. (1983) with MODIS-observed radiances within the 15 μm carbon dioxide absorption band (Platnick et al. 2003). This method is most effective for mid- to high-level clouds, but for clouds with tops below 700 hPa the signal to noise ratio is poor. For these low clouds, the retrieval is performed using only the 11 μm brightness temperature, under the assumption that the cloud is sufficiently thick to prevent interference from surface emissions. The production of the level two data additionally involves the use of a cloud mask to screen for cloud presence, which is especially relevant to the study of orographic clouds as the cloud top temperatures may not differ greatly from the temperature of the surrounding terrain.

The development of sophisticated satellite instrument simulators is a topic of ongoing interest, for example Otkin and Greenwald (2008) used a radiative transfer model to calculate top-of-atmosphere brightness temperatures from WRF numerical output, and passed these through the MODIS algorithms to evaluate the model simulations against MODIS observations. Such approaches are especially useful for interpreting the observations of the instruments themselves, but for the purposes of this case study a simpler approach was taken. We used the ambient temperature at an optical thickness of $\tau = 0.5$ from the top of the model domain as a proxy for the cloud top temperature. This value was found to be a good balance in capturing the features of the optically thin cold cloud while not affecting the representation of low-level clouds. Optical thickness was calculated based on absorption of visible light by hydrometeors, specifically cloud water, ice, snow, and rain as per Dudhia (1989).

The scenes in Fig. 7 show the cloud top temperature as viewed by the MODIS instrument and simulated by the WRF model at two moments in the July case study period. The first overpass occurred while the frontal band was overhead, with a striated double-band of cold cloud evident in the MODIS imagery. Overlying this in the upper right corner is an even colder streak associated with the strong jet stream. Both of these features, as well as the fractional low-level coverage, are quite well-represented by the WRF diagnostic, which was performed on the 12.15 km domain, but the optically thin cloud streak was found to be sensitive to the threshold of τ chosen.

The second MODIS retrieval shows a tongue of cold cloud which forms the leading edge of the 'wrap-around' feature evident in the MSLP-IR composite analysed at about the same time (not shown). We speculate that this may be a result of the occlusion, but in any case this complex dynamical feature appears to be less well simulated by the WRF model. We found that this feature was highly sensitive to the threshold of τ selected, with lower values giving a

Fig. 5. Wagga Wagga sounding (darker line) alongside WRF simulated atmospheric profile (lighter line) for the July case. These soundings were taken at 0000 UTC 20 and 21 July, and represent the pre-frontal and post-frontal conditions. The WRF profiles presented are those nearest matching the observations at 0000 UTC 20 July and 2300 UTC 20 July.

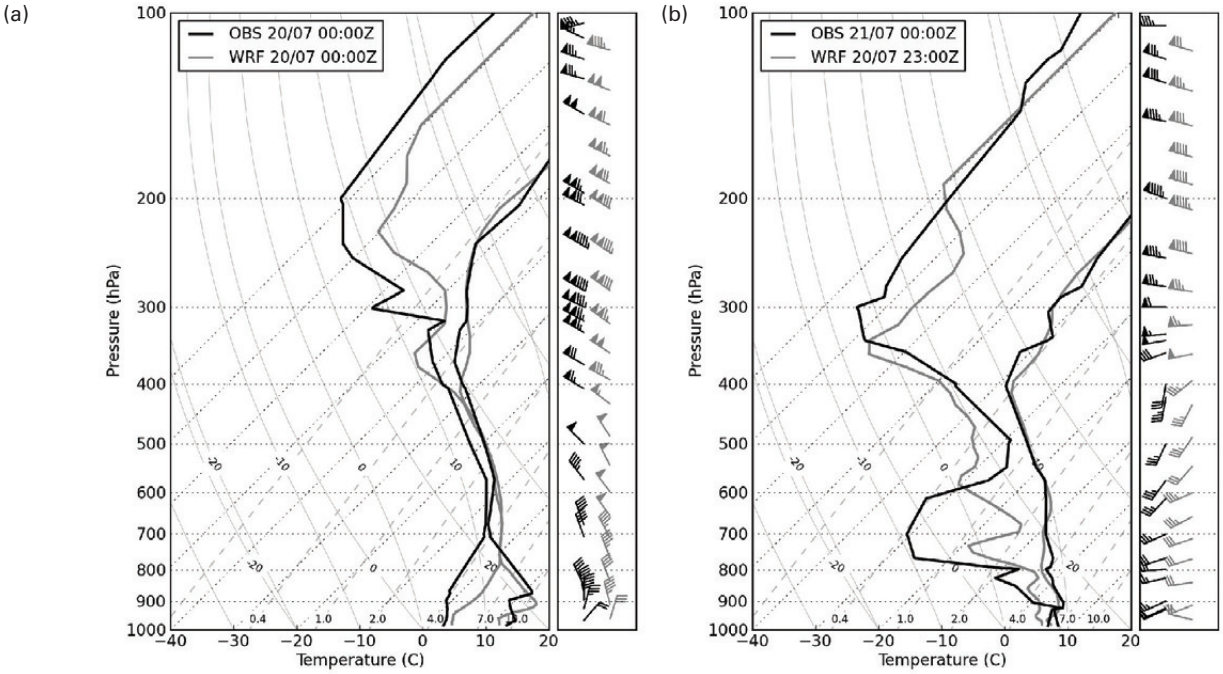

Fig. 6. As for Fig. 5, but for the August case. No pre-frontal sounding was made, so only the simulated profile at 1800 UTC 9 August is shown. The post frontal sounding was made at 1200 UTC 10 August, and the simulated profile for 1000 UTC is shown for comparison.

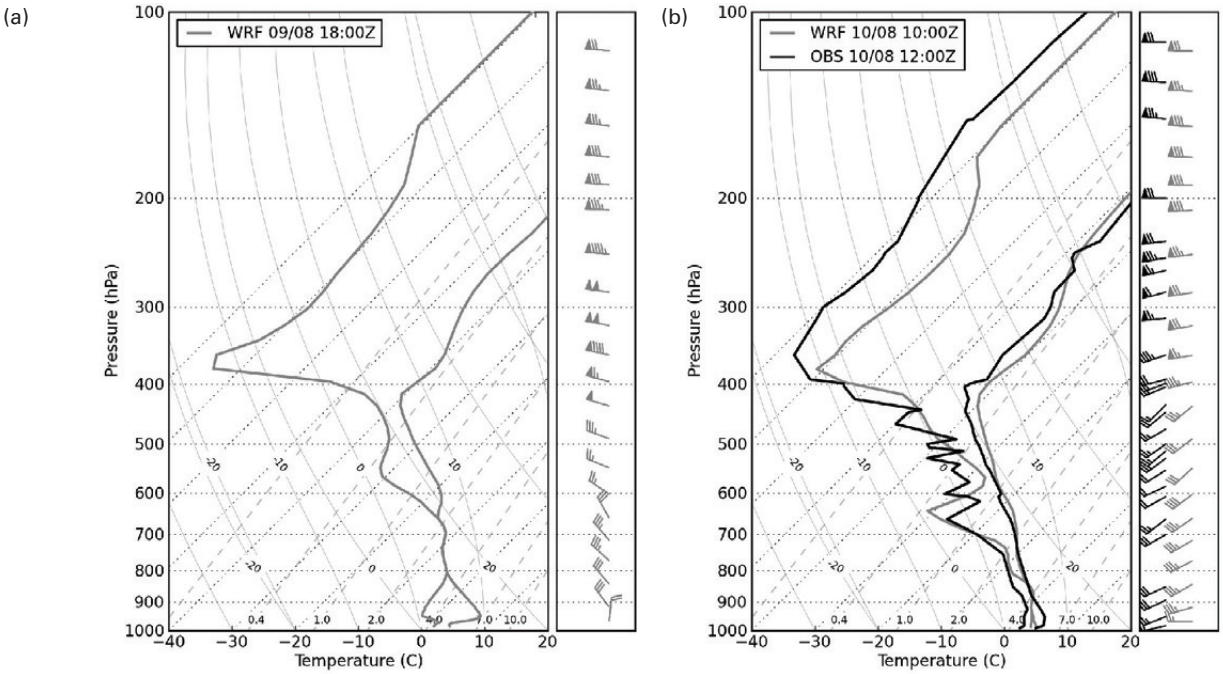

Fig. 7. MODIS retrievals of cloud top temperature for 0410 UTC 20 July and 0035 UTC 21 July (left panels), and corresponding WRF retrievals (right panels). The WRF cloud top temperatures were calculated by vertically integrating optical thickness to a value of $\tau = 0.5$ using hydrometeor extinction coefficients from literature (see text). The cold cloud in the lower panels is optically thin and the WRF retrieval is sensitive to the threshold of τ selected.

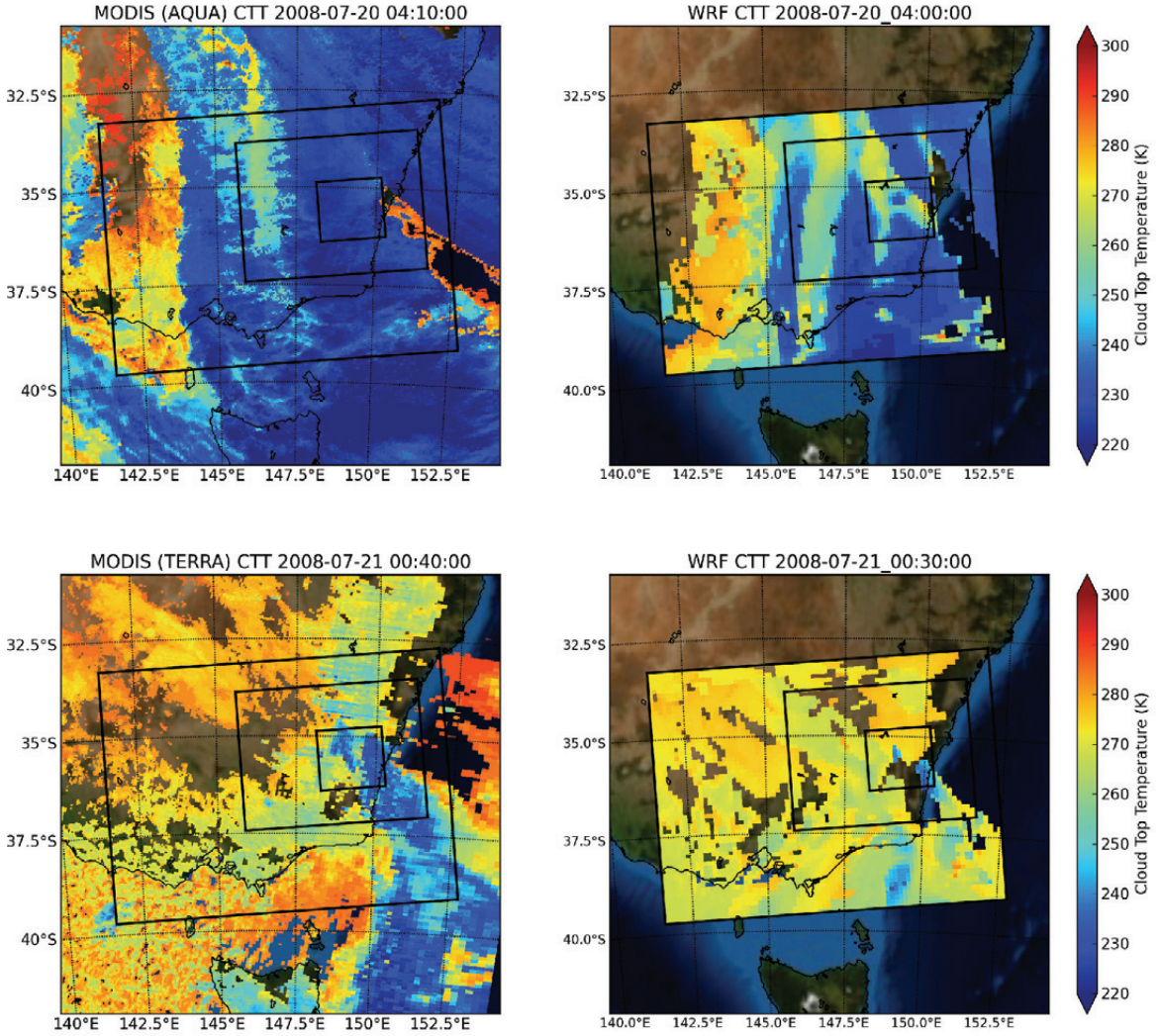

better representation at the expense of displaying cirrus cloud not observed by MODIS. Low-level clouds with tops around –13 °C at several points along the GDR are apparent in both the MODIS retrieval and the WRF diagnostic at this time, with the model showing somewhat greater areal coverage, and are persistent during the post-frontal period for the WRF simulation.

A scene roughly coinciding with the frontal passage during the August case study is presented in Fig. 8, occurring very close to the analysis time shown in Fig. 3. The WRF representation of the frontal band at a simulation time of 2230 UTC (consistent with the dynamical offset) is again quite remarkable, but the cold cloud features associated with the centre of circulation are slightly displaced. The representation of the post-frontal scene is quite reasonable, but again depicts higher than observed areal coverage of low cloud.

Captains Flat radar reflectivity

The Captains Flat (Canberra) weather radar gives good coverage of the analysis region above altitude 3000 m, but below this level the data is affected by terrain blocking and curvature effects, as the radar is located some 70 km away. Figures 9 and 10 show contoured frequency by altitude (CFAD) representation of the radar reflectivity in the analysis region during the two 12-hour intervals for the two cases. The contours represent the absolute frequency of observing reflectivity of a certain value at a given altitude. The contour intervals are quadratically spaced to enhance the tails of the distributions. To investigate the influence of the topography, the analysis region was split longitudinally into two equal parts, roughly along the main ridge line of the Brindabella Ranges, and CFADs for each half are depicted. For both cases, the winds were predominantly westerly, so the left panels were 'upwind' of the ranges.

During the frontal period of the July case (top panels of

Fig. 8. MODIS retrievals of cloud top temperature for 0015 and 1535 UTC 10 August, and corresponding WRF retrievals (right panels—note that there was some 'lead' in the WRF simulations).

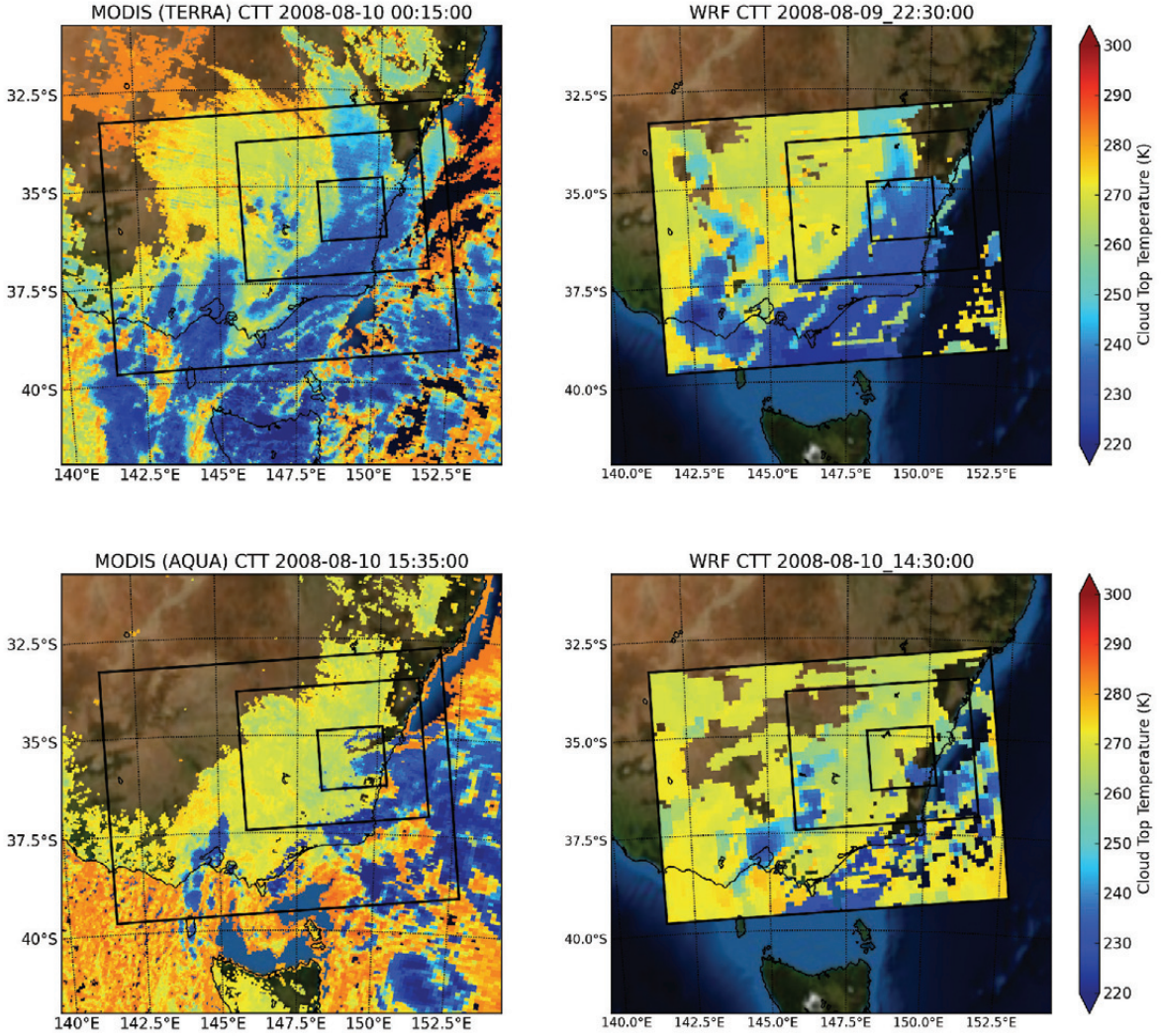

Fig. 9), the CFAD representations are quite similar east and west of the ranges, with peak reflectivity of about 40–45 dBZ and echoes recorded up to 8 km. There was no significant difference in the total number of pixels recording an echo (total counts). Our interpretation of these CFADs is that the precipitation structure was similar upwind and downwind of the ranges during this dynamically dominated interval.

In contrast, there are substantial differences between the upwind and downwind CFADs during the post-frontal interval of the July case study. The primary difference is in the total number of echoes recorded, with about three times the frequency upwind of the ranges. The modal reflectivity was slightly higher for the upwind CFAD, and echoes were recorded to higher altitudes, indicating more developed precipitation structures upwind. The influence of the topography during the post-frontal phase of this case is clearly important.

The less intense August case shows a different pattern (Fig. 10), in which both the frontal and post-frontal phase have markedly different upwind and downwind reflectivity CFADs. In both intervals, the modal reflectivity was higher and echoed were recorded to higher altitudes for the upwind CFADs. Echoes were about three times as frequent in the upwind part of the analysis region during the frontal interval, and about six times as frequent in the post-frontal interval. The downwind part of the analysis region could be characterised as essentially non-precipitating during the post-frontal phase. The topography of the Brindabella Ranges clearly has a controlling influence over precipitation throughout this less dynamic case.

Surface observations and precipitation patterns

Mountain top AWS observations at Mt. Ginini (Fig. 11) show a gradually increasing temperature overnight on 19 July, reaching a maximum of 3.5 °C at about 0100 UTC (1100 AEST), with sustained wind speeds of up to 40 km hr^{-1} from the north. Both the WRF model simulations and the

Fig. 9. Contoured frequency by altitude diagrams (CFADs) for Captains Flat radar reflectivity for the two intervals considered during the July case. The analysis region was divided longitudinally into two parts to examine differences in precipitation structure upwind (left panels) and downwind (right panels) of the Brindabella Ranges.

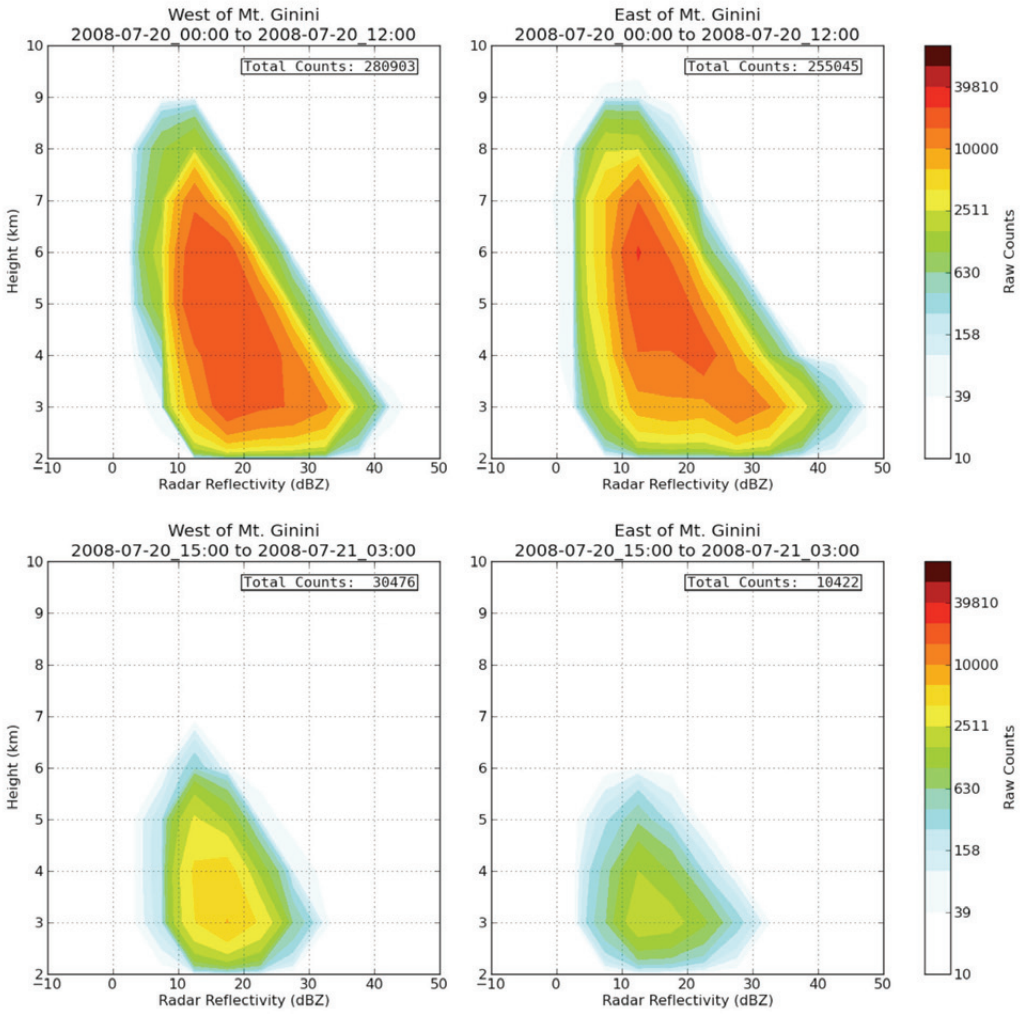

observations showed a distinct, temporary wind direction change roughly coincident with the onset of precipitation, but in the simulation this occurred several hours before the observations. The simulated temperature dropped below the observations between 0400 and 0900 indicating cold air advection during the westerlies. The heaviest simulated precipitation (up to 15 mm hr^{-1}) occurred during this period, and was enhanced by the strong cross-barrier component of the winds. In both the simulations and the observations, winds returned to northwesterly momentarily before gradually turning southwesterly over the subsequent 24 hours, which were characterised by cloudy conditions and persistent light precipitation (about 1.2 mm hr^{-1} for 16 hours).

At Wagga Wagga, as for Mt. Ginini, a wind directional change was associated with the onset of precipitation, and this occurred slightly earlier in the simulation. Conditions were apparently quite calm at Isabella Plains when precipitation started, but a slight wind shift was simulated. At both of these sites precipitation had virtually ceased by the end of the 'frontal' interval. The temperature towards the end of the analysis period indicates a return to clear conditions at Wagga Wagga and Isabella Plains, with a well-defined diurnal cycle apparent at both sites. The low-level winds are also better simulated during the second half of the analysis period, but the simulated temperatures were a little colder than observed, possibly due to the excess low-level cloud identified in Fig. 7 during this period.

Conditions during the August case were considerably cooler at all three sites (Fig. 12), and as a consequence of the less intense dynamics, the variation in temperature and wind was better simulated. Only a weak directional change was apparent in the winds at Mt. Ginini at around 2200 UTC 09 August, and the simulations lagged slightly in agreement with the differences in timing noted above. The simulated surface winds were somewhat stronger than the observations, which was also the case in the post-frontal sounding at 1200 UTC on 10 August. Two distinct periods of precipitation were observed at Mt. Ginini, the first coinciding with the wind shift, and the second with a slight decrease in temperature at around 0200 UTC 10 August,

Fig. 10. As for Fig. 9, but for the August case.

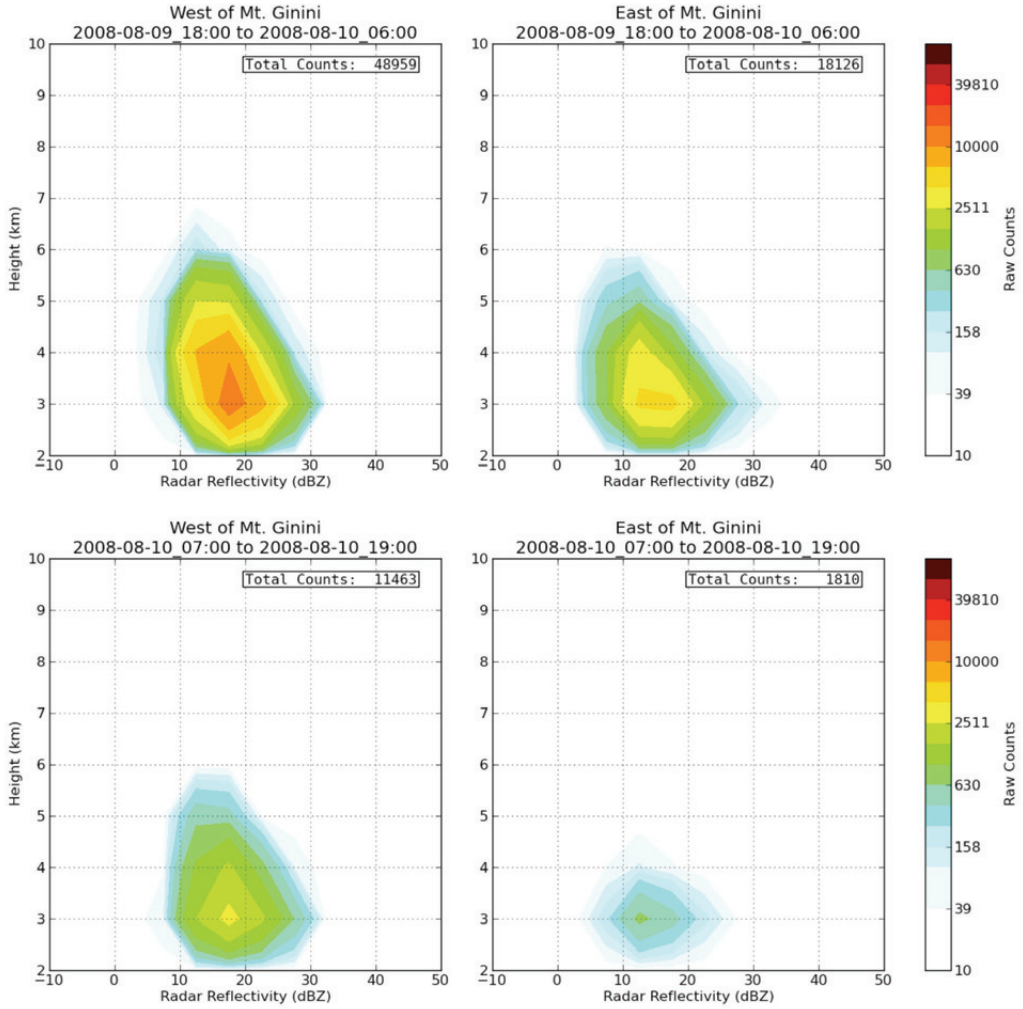

with only slight precipitation recorded after this. The WRF simulations under-predict precipitation in the first interval (a) but excess gradual precipitation in the second interval (b) brings the total for the storm to about the same amount as the observations.

Precipitation associated with the front was well-forecast at Wagga Wagga, where some 8 mm was recorded. During the post-frontal interval, very little precipitation was recorded, but the simulations predicted an additional 12 mm gradually accumulating—more than was predicted at Mt. Ginini in the same time. Very little precipitation was recorded at Isabella Plains during this event.

Figure 13 shows the 24-hour precipitation to 0900 AEST for the WRF model domains four and five in the analysis region centred on Mt. Ginini, as well as the 24-hour precipitation amounts recorded by the nearby Bureau of Meteorology gauges. We used an inverse distance weighting method to interpolate the simulated precipitation field onto a 0.05 × 0.05° grid, and to put the precipitation patterns near Mt. Ginini in context, a larger region is shown in these figures. The terrain is shown as represented in the WRF simulations.

Precipitation patterns in the July case show a clear orographic signal, with maxima located near prominent topographical features. The gauge values agree fairly well with the simulation results, except in the elevated terrain to the southwest of the analysis region. The impact that the horizontal resolution has on these results is profound, in particular where the terrain is steep and complex. The ridge line representing the Brindabella Ranges along the western border of the Australian Capital Territory is poorly defined in domain four, and the precipitation enhancement associated with it is weak. It is much more prominent in domain five, and the precipitation enhancement is correspondingly much clearer. Interestingly, the principal enhancement is slightly downwind of the ranges (note that one grid cell in this figure has about three times the width of a domain five grid cell). This effect is apparent near other prominent topographic features as well, e.g. the steep terrain representing one side of the Tumut River valley, to the west of the analysis region. This 'spillover' effect is a well-documented feature of orographic precipitation (Sinclair et al. 1997), and tends to occur in strong or unstable flow conditions.

Fig. 11. Surface meteorological variables observed (circle markers and coloured barbs) and simulated (square markers and grey barbs) at each of the automatic weather stations. The precipitation amounts shown are smoothed from the WRF grids using a 5 × 5 grid cell window, and temperatures at Mt. Ginini are adjusted for station elevation. As in the text, two 12-hour intervals are indicated showing the frontal (a) and the post-frontal (b) conditions. Note that the Wagga Wagga AMO is situated outside the highest resolution domain.

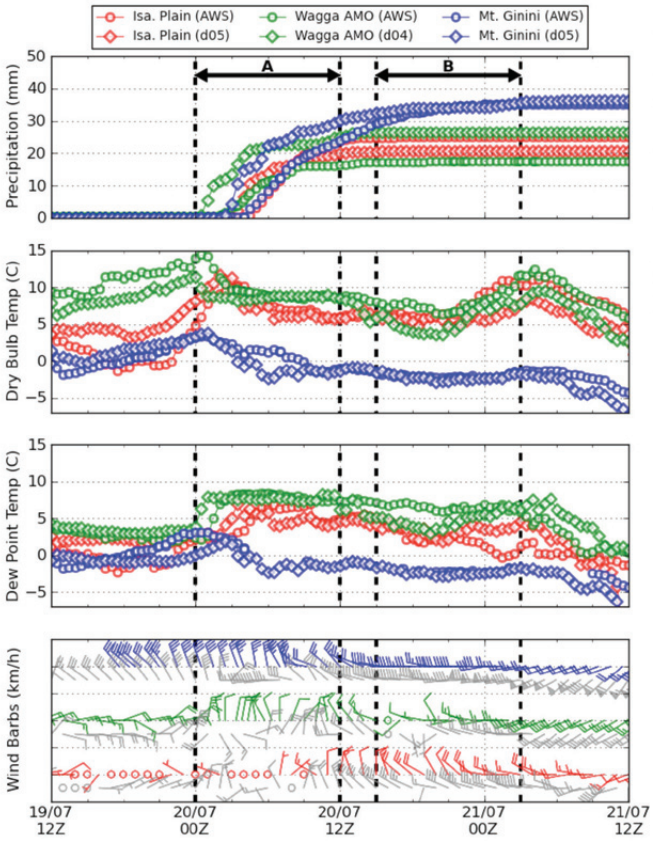

The August case shows a distinctly different pattern of precipitation. Firstly, an explanation for the relatively low post-frontal precipitation recorded during this storm is that it may have principally occurred upwind of Mt. Ginini. Time series of simulated precipitation amount (not shown) on the lower western slopes support this, with substantial precipitation falling in interval B, but without suitable AWS data it is hard to verify this speculation. Indeed, variability in the daily gauge data is conspicuously lacking, with nearly all sites recording about 5–15 mm. However, it is likely that these gauges underestimate frozen precipitation in elevated regions in this much colder case. An independent gauge network with specialised all-season gauges in the Snowy Mountains recorded as much as 30 mm on the same day, agreeing with the magnitudes suggested by the WRF model for that region (lower left corner in this figure). The higher resolution domain does not add much structure to the spatial distribution of precipitation, suggesting lower sensitivity to spatial resolution for this case.

Fig. 12. As for Fig. 11, but for the August case.

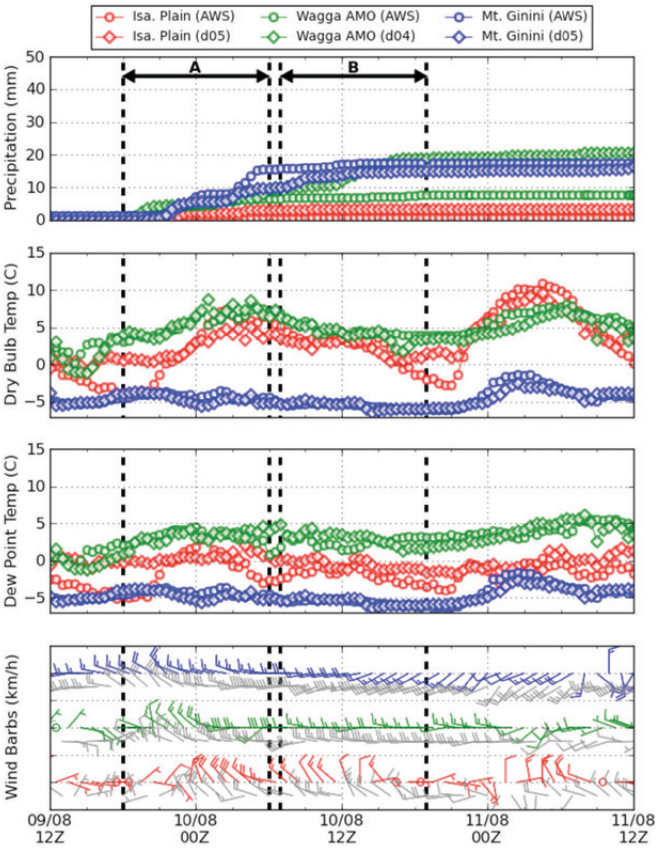

Remotely sensed observations from Mt. Ginini

Cloud liquid water path (LWP) and water vapour path (WVP) can be evaluated by measuring atmospheric brightness temperature at a pair of frequencies in the microwave band (Westwater 1978). These are selected to coincide with the peak absorptivity and the window region for water vapour (around 22.2 and 30 GHz respectively), and from the differences in the absorptivity at these frequencies the column integrated values can be determined (Gaussiat et al. 2007). Uncertainty results from variation of the absorption coefficients for liquid and vapour, which are temperature and pressure dependent. This is mitigated operationally by performing regular 'calibration tips' when clear sky radiances are available, but estimates of measurement uncertainty for LWP are typically in the region of 0.02 kg m^{-2}.

The MODIS instrument also provides a cloud water path (CWP) observation determined from cloud optical thickness τ_c and cloud particle effective radius r_e, using the following relation (Stephens 1978):

$$\mathrm{CWP} = \frac{4\rho\tau_c r_e}{3Q_e}, \qquad \ldots(1)$$

where ρ is a density parameter (1.0 for liquid, 0.93 for ice), and Q_e is the extinction efficiency (about 2 for visible wavelengths). The limitations of this method are that it

Fig. 13. Gridded 24-hour precipitation amount for the July case (a) and the August case (b). The left and right panels show WRF simulations of precipitation amount from domains four and five respectively, interpolated onto a 0.05 degree grid. Note that the domain five boundary falls within the depicted region. The coloured dots show observations from the Bureau of Meteorology's daily precipitation network.

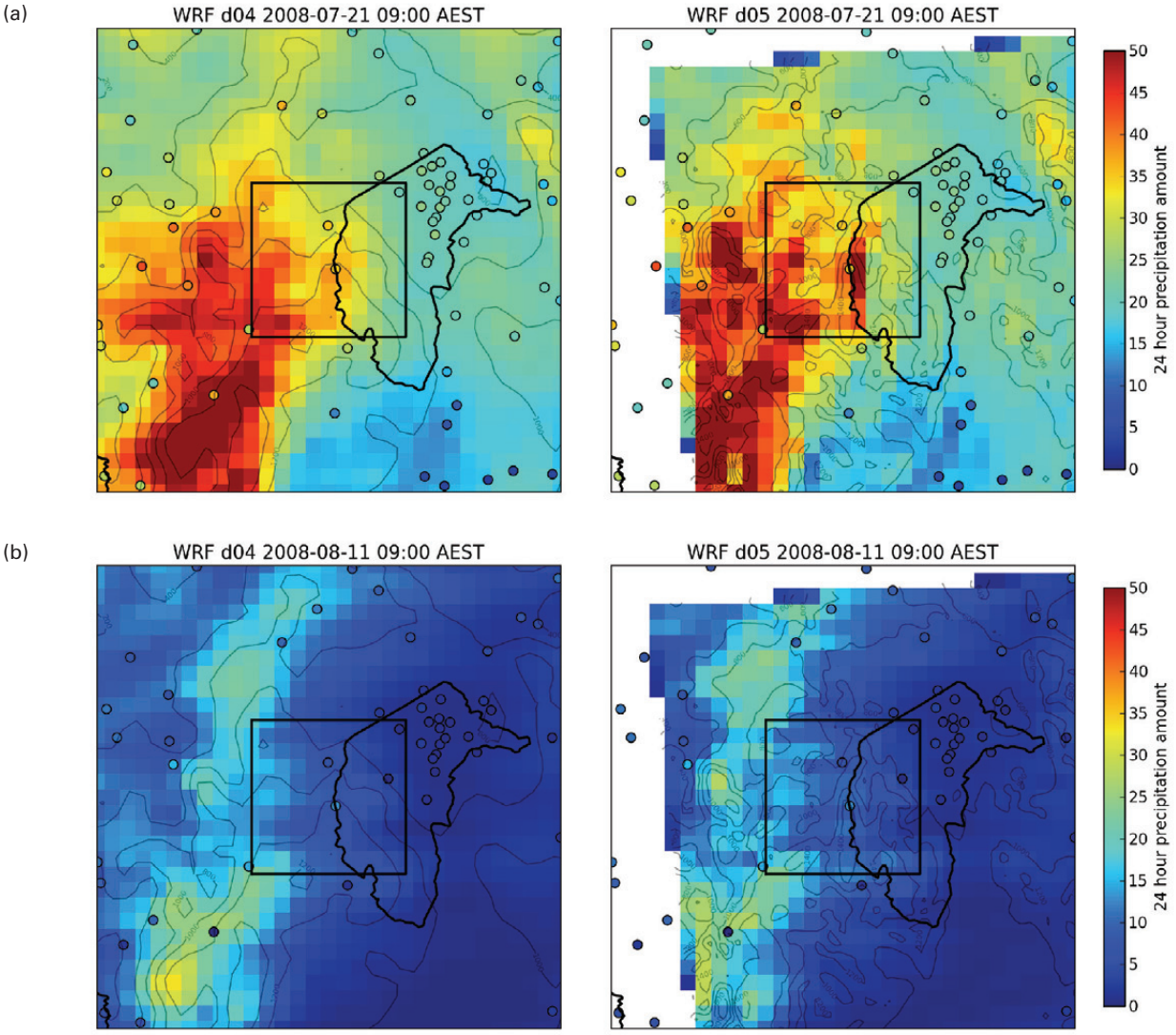

assumes the same r_e and phase for the entire column as for cloud top. (Horváth and Davies 2007) compared MODIS CWP with satellite-based microwave radiometer estimates, finding good agreement (overall correlation coefficient 0.85 with an RMS difference of 0.025 kg m^{-2}).

Cloud LWP and WVP above Mt. Ginini were calculated from the dual-channel microwave observations in this manner and are displayed for the two case studies in the upper panels of Figs. 14 and 15. The one-minute time series data was under-sampled to match the periodicity of the WRF model output (15-minutes), and the error bars show one standard deviation for the radiometer data in a 15-minute window centred on the observation time. Also plotted over the time series are box plots of the available data from the MODIS overpasses, showing the CWP median and interquartile range, as well as the 90th percentiles, for the 0.25° box centred on Mt. Ginini.

For the simulations, column-integrated values for liquid water and water vapour are calculated from liquid hydrometeor (cloud water and rain), and water vapour mixing ratios at the nearest grid point, and are shown in the middle panels of Figs. 14 and 15. The variability of the LWP and WVP in a 5 × 5 grid cell column is displayed by the error bars as a substitute for high frequency temporal variability. The lower panels of Figs. 14 and 15 show quantile–quantile plots (specifically five percentile values), to compare the distributions of WVP and LWP for each of the 12-hour intervals.

For the July case, increasingly high values of WVP were observed until shortly after the frontal passage, coinciding with a period of high LWP values (around 1.4 kg m^{-2}), as well as the highest surface precipitation rates at Mt. Ginini. Conditions at the Mt. Ginini AWS were above freezing for most of this interval, so it is likely that precipitation was

Fig. 14. Observed (top panel) and simulated (second panel) radiometer measurements, and Q–Q plots comparing the distributions of column-integrated water vapour and liquid water (lowest panels). The radiometer data is under sampled to match the 15-minute period of the WRF output, and the variability for this period (1–σ) is shown by the error bars. Statistics for MODIS observations of cloud water path for a 0.25° box centred on Mt Ginini are represented by the box plots over the observed time series (90th percentiles shown by whiskers). The quantile–quantile plots in the lower panels compare vigintiles, (5-percentiles) for the 12-hour intervals A and B.

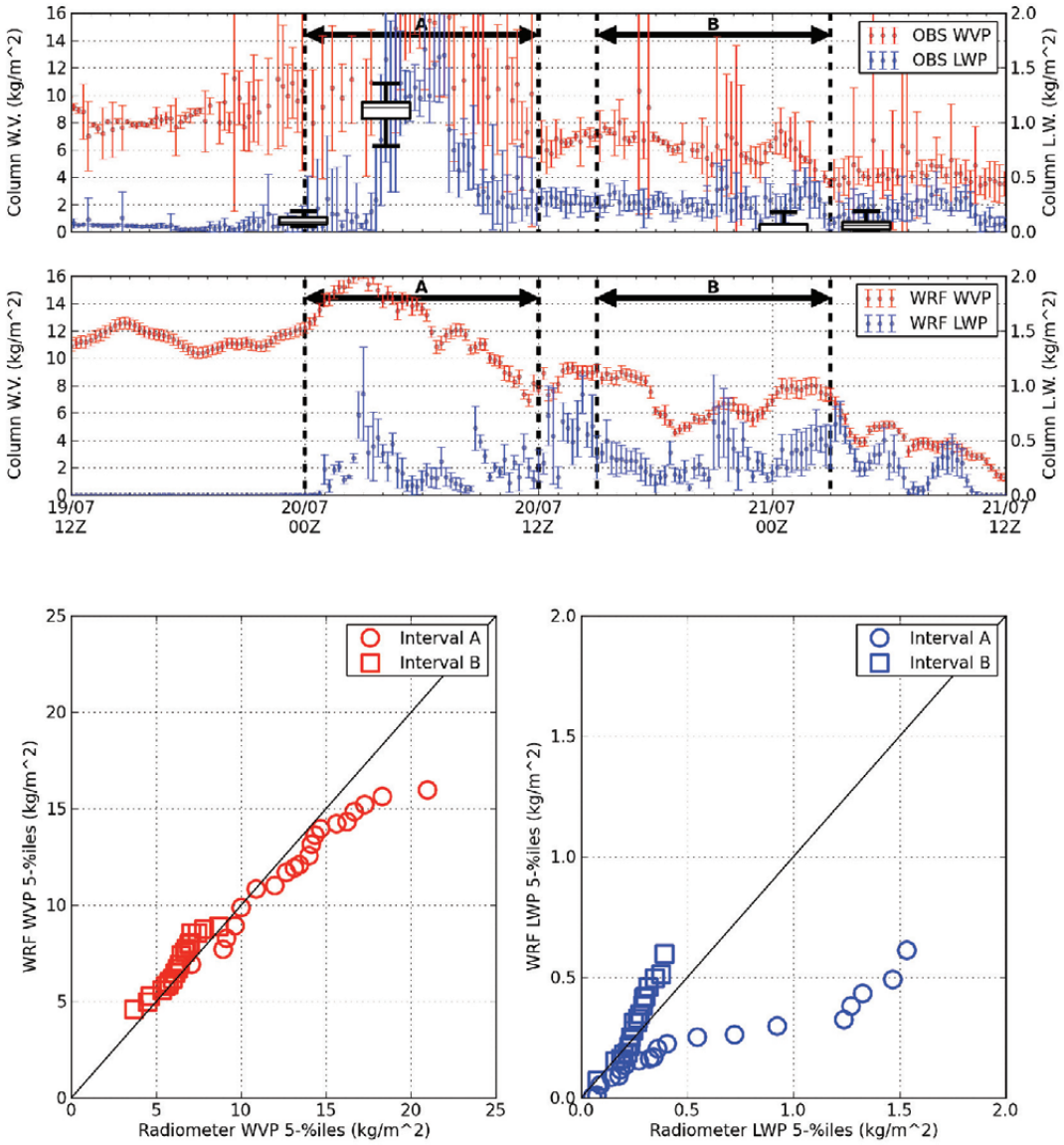

falling as rain or mixed rain and snow.

Droplet collection on the radiometer microwave window during heavy rainfall is a known cause of erroneously high values for LWP, but good agreement is nevertheless shown between the surface-based and MODIS retrievals for this period. However, this comparison is treated cautiously given the limitations of the MODIS retrievals in the deep, heterogeneous cloud of the frontal band. A speculative interpretation of the large discrepancy between the observed and simulated LWP values is that the microphysics scheme of the WRF model may be simulating the production of precipitation too rapidly during this period through conversion of liquid water to ice hydrometeors, which would explain both the lower LWP amounts as well as the higher precipitation rate during the onset of precipitation, but without in-cloud microphysical observations this hypothesis is impossible to investigate further.

The statistics during the two indicated 12-hour intervals differ in accord with the different dynamic phases of the storm. The first period is roughly centred on the time of the frontal passage, and the median value for observed WVP is about 14 kg m^{-2}. The WRF simulations represent the distribution of the WVP values relatively well, but slightly under predict the upper quartile. The median observed LWP values were about 0.36 kg m^{-2} compared to simulated values of about 0.20 kg m^{-2}, and the upper half of the distribution is

Fig. 15. As for Fig. 14, but for the August case.

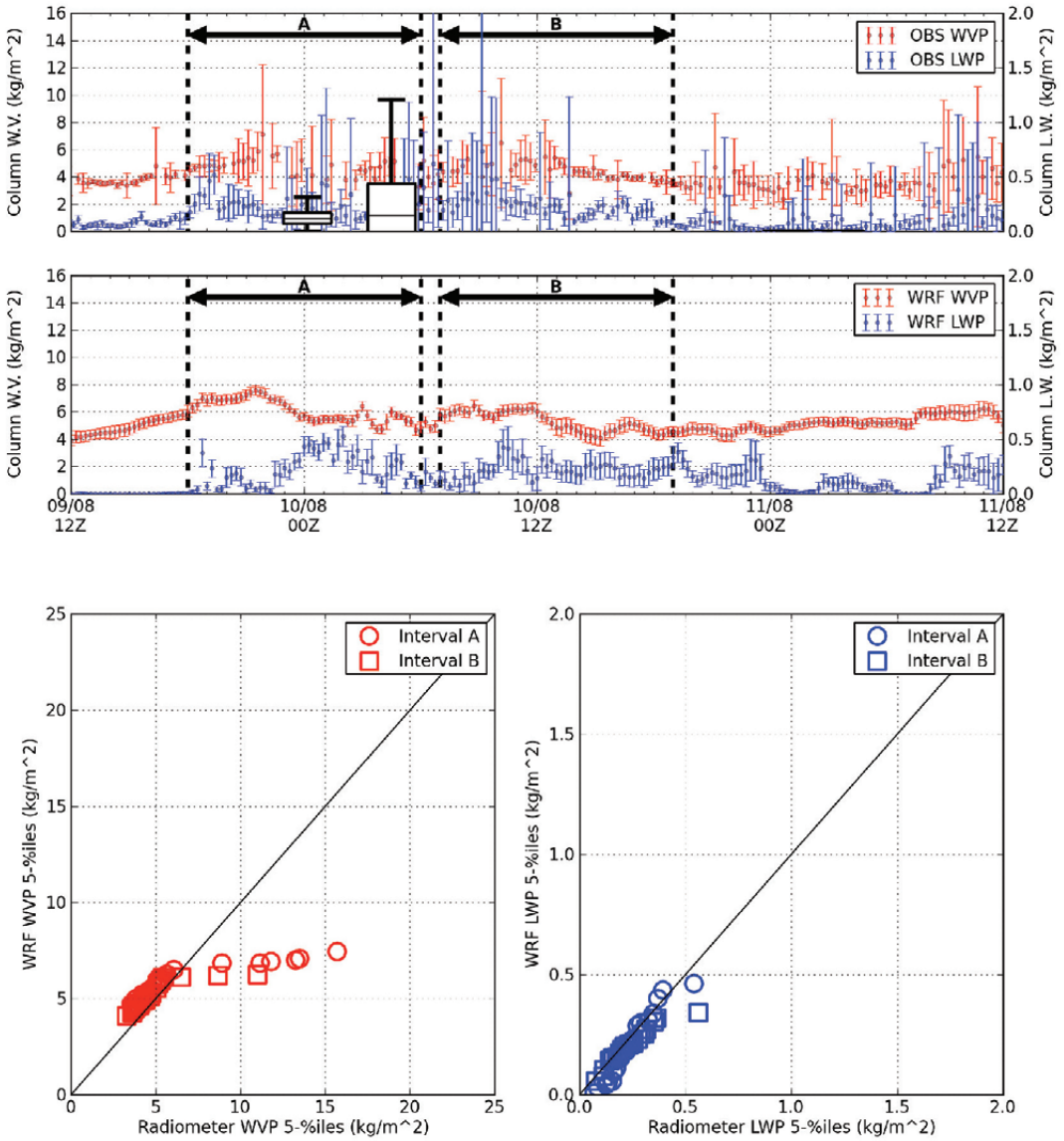

very poorly represented by the simulations.

During the second 12-hour interval, the median simulated LWP values were very similar to the observations, with values of 0.31 and 0.27 kg m^{-2} respectively. The variability of the LWP in this interval is very low, and the temperature is below freezing during this entire interval, indicating persistent supercooled liquid water over the ranges.

The August case study is characterised by lower observed WVP values (typically 4–8 kg m^{-2}), which, together with the lower wind speeds for this event, imply that the water vapour flux for this case was lower. There is little variation over the course of the case study period, corresponding to the weaker dynamical forcing in this case. Cloud LWP values are lower than for the July case, but also highly variable, reaching above the background level of 0.05 kg m^{-2} shortly before the frontal passage, and persisting for about 30 hours. MODIS retrievals again show very good agreement with the radiometer near 0000 UTC, but for 0400 UTC there is very high spread in the satellite data, reflecting the variability on small scales of the cloud in this mountainous region.

The simulated WVP again tracks the observations quite closely, although there is a systematic bias of about 0.1 kg m^{-2} , or about 20 per cent, evident in the distributions shown in the lower panels. Extreme values of WVP are not captured by the WRF model, but it is not clear if this is an artefact of the data or a consequence of the implicit smoothing due to numerical discretisation.

The simulated cloud LWP values do not follow the observations temporally, but the cloudy duration at Mt. Ginini is about the same. The distribution of simulated values is quite well simulated for both of the 12-hour periods, with less than 20 per cent error in the median LWP for both intervals, so it may be inferred that the cloud 'populations' are again well-represented.

Discussion and summary

Performance of the WRF model in simulating alpine wintertime storms

The primary objective of this paper was to assess the performance of the WRF model in simulating wintertime storms in an alpine environment with complex topography, with a particular focus on the representation of clouds and precipitation. The use of a case study approach allows for the evaluation of the model in the context of the synoptic conditions of interest. The two events offer some contrast in that the July event was characterised by a strongly dynamic cut-off low, while the August event was a weaker, less well organised system with a complex of frontal bands. Both events were followed by an extended post-frontal period, characterised by shallow, liquid phase clouds and light precipitation sustained for at least 12 hours.

The broadscale meteorology was assessed through a basic comparison of atmospheric profiles from a location upwind of the primary analysis region. Differences in timing were identified that corresponded to offsets in the timing of changes in the surface meteorological data and cloud top retrievals. In both case studies it was noted that excessive moisture was present in the lower levels of the profiles. Both of these differences can be caused by errors in the data used to generate lateral boundary conditions, but further work, including the use of different surface a planetary boundary layer conditions, could be performed to establish this.

The representation of cloud structure in the broader region was evaluated through comparison of cloud top temperatures from the MODIS instrument with an ad-hoc diagnostic based on simulated hydrometeor mixing ratios. Good agreement was found between the simulations and observations, but the representation of simulated cold, thin clouds was found to be quite sensitive to the optical thickness threshold used to define 'cloud top'. In both cases, too much low-level cloud was simulated in the post frontal scenes. This is most likely connected to the excess moisture simulated in the lower levels of both cases.

Surface meteorological conditions were evaluated by comparing the simulations to half-hourly data from three automatic weather stations and a large number of daily precipitation gauges operated by the Bureau of Meteorology. The most notable discrepancies were the excessive post-frontal precipitation simulated at Wagga Wagga in the August case, and the over-prediction of precipitation (relative to the daily gauge data) along the western slopes of the GDR in both cases. The latter of these discrepancies is the most pressing for the use of WRF as a forecast model in the mountainous regions. We note that the use of daily precipitation data from alpine regions to evaluate the simulations is flawed, as it is likely to severely under-represent frozen precipitation in high wind conditions. A more comprehensive analysis of precipitation simulations in the Brindabella Ranges would be futile without investment in an improved observational network, such as has been developed in the Snowy Mountains region by Manton et al. (2011).

An interesting result of this study was the striking agreement between the radiometer integrated liquid water path and the simulated values, in spite of the discrepancies in surface precipitation. Aside from the frontal interval during the August case—which was poorly represented due to either dominance by ice precesses in the model or influence of raindrops on the radiometer data (or perhaps both)—both the distribution of LWP values and the cloudy duration was well represented. The persistence of these clouds observed by the radiometer adds support to the findings of Morrison et al. (2011) that supercooled cloud tops are frequently observed along the GDR.

Implications for future cloud seeding research in the Brindabella Ranges

Following the success of recent cloud seeding efforts in the nearby Snowy Mountains region (Manton et al. 2011), it is tempting to extrapolate these results to the Brindabella Ranges, which are nearby and have a similar elevation. There are, however, a number of practical considerations to account for when designing a cloud seeding operation, experimental or otherwise. The most important of these are:

- Persistent and frequent occurrence of supercooled liquid clouds;
- Effectiveness of topographical barrier at modifying meteorological conditions;
- Suitability of upwind terrain for installation of ground-based generators that will effectively target the analysis region or accessibility for aircraft operations;
- Suitability of precipitation gauge network to evaluate impact of cloud seeding operations;
- Existence of effective control regions to evaluate impact of cloud seeding operations; and
- The prospect of using numerical models to test the hypotheses of glaciogenic cloud seeding.

The analyses performed for this paper do not attempt to answer all of the above considerations; rather they illustrate conditions typical of wintertime storms in this region.

The radiometer data provide the strongest support for the possibility of conducting cloud seeding experiments in the Brindabella Ranges. During both of the storms persistent supercooled liquid water was present above Mt. Ginini, in quantities well in excess of the minimum value of 0.05 kg m^{-2} required to commence cloud seeding experimental units in the Snowy Mountains, as described in Manton et al. (2011). This study does not address the issue of frequency of occurrence of such conditions. To do this, season-long (preferably multiple seasons) analyses would have to be performed.

The radar reflectivity data from Captains Flat show that in both of the case study storms, the Brindabella Ranges substantially modified the structure of precipitation. More echoes, with peak occurrences at higher intensity and elevation, were seen on the western (upwind) side of the ranges in all intervals except for the dynamically-dominated frontal interval in the July case.

The evaluation of the simulated surface precipitation was deficient in this study due to the lack of good quality observations in the Brindabella Ranges. As surface precipitation is the primary response variable of a cloud seeding trial, the observational network would need to be substantially upgraded to support any further investigation.

An unexpected outcome of the simulations was the finding that substantially more precipitation occurred on the lower mountains located upwind of the Brindabella Ranges. These are important because they are the first substantial topographic feature to westerly flow over the Murray-Darling Basin, and examination of the broader-scale mean wintertime (May–September) rainfall (NCC 2012), shows that the Brindabella Ranges are indeed on the downwind side of the maximum precipitation belt of the GDR. If precipitation amounts during wintertime storms are modulated by upwind features, it could impair the detection of any signal due to cloud seeding efforts.

Ryan and King (1997) noted that numerical models were a promising prospect for testing cloud seeding hypotheses, but that gaps in the understanding of ice generation in clouds limited their use. There has been considerable advance in the use of numerical models in cloud seeding experiments since this review, for example Lulin et al. (in press 2012) recently implemented a full treatment of glaciogenic cloud seeding into the WRF model by modifying the Thompson et al. (2004) microphysics scheme. The performance of the WRF model in simulating cloud LWP demonstrated by the case studies presented in this paper lends weight to arguments for the use of numerical models in the evaluation of cloud seeding experiments. One of the primary hypotheses of glaciogenic cloud seeding is that the introduction of ice nuclei into primarily supercooled clouds results in the depletion of liquid water as snowflakes grow. This has been shown empirically in the Snowy Mountains experiments (Manton and Warren 2011), and could readily be tested by statistical treatment of radiometer data and WRF simulations for a randomised trial.

Acknowledgements

The authors acknowledge ActewAGL for provision of funding for this work. Ian Hampton and Melanie Wetzel collected and processed the radiometer data used in this analysis, and the Australian Bureau of Meteorology produced the mean sea-level pressure analyses and radar data used in this paper. This paper has benefited from the insightful comments of two anonymous reviewers.

References

Boers, R. and Krummel, P.B. 1998. Microphysical properties of boundary layer clouds over the Southern Ocean during ACE 1. *J. Geophys. Res., 103,* 16651–64.

Chubb, T.H., Siems, S.T., and Manton, M.J. 2011. On the decline of wintertime precipitation in the Snowy Mountains of South-Eastern Australia. *J. Hydrometeor., 12* (6), 1483–97.

Dudhia, J. 1989. Numerical Study of Convection Observed during the Winter Monsoon Experiment Using a Mesoscale Two-Dimensional Model. *J. Atmos. Sci., 46,* 3077–107.

Gaussiat, N., Hogan, R.J., and Illingworth, A.J. 2007. Accurate Liquid Water Path Retrieval from Low-Cost Microwave Radiometers Using Additional Information from a Lidar Ceilometer and Operational Forecast Models. *J. Atmos. Oceanic Tech., 24,* 1562.

Horváth, A. and Davies, R. 2007. Comparison of microwave and optical cloud water path estimates from TMI, MODIS, and MISR. *J. Geophys. Res., 112,* D01 202.

Janjić, Z.I. 1994, The Step-Mountain Eta Coordinate Model: Further Developments of the Convection, Viscous Sublayer, and Turbulence Closure Schemes. *Mon. Weather Rev., 122,* 927.

Landvogt, P., Bye, J., and Lane, T. 2008. An investigation of recent orographic precipitation events in northeast Victoria. *Aust. Meteorol. Mag., 57.*

Larsen, S.H. and Nicholls, N. 2009. Southern Australian rainfall and the subtropical ridge: Variations, interrelationships, and trends. *Geophys. Res. Lett., 36,* L08 708.

Lulin, X., et al., in press 2012: AgI cloud seeding effects as seen in WRF simulations. Part I: Model description and idealized 2D sensitivity tests. *J. Appl. Meteorol. Climatol.*

Manton, M.J. and Warren, L. 2011. A Confirmatory Snowfall Enhancement Project in the Snowy Mountains of Australia. Part II: Primary and Associated Analyses. *J. Appl. Meteorol. Climatol., 50,* 1448–58.

Manton, M.J., Warren, L., Kenyon, S.L., Peace, A.D., Bilish, S.P., and Kemsley, K. 2011. A Confirmatory Snowfall Enhancement Project in the Snowy Mountains of Australia. Part I: Project Design and Response Variables. *J. Appl. Meteorol. Climatol., 50,* 1432–47.

Mellor, G. and Yamada, T. 1982. Development of a turbulence closure model for geophysical fluid problems. *Rev. Geophys. Space Phys., 20,* 851–75.

Menzel, W.P., Smith, W.L., and Stewart, T.R. 1983. Improved Cloud Motion Wind Vector and Altitude Assignment Using VAS. *J. Appl. Meteorol., 22,* 377–84.

Morrison, A., Siems, S., and Manton, M., 2011. A Three-Year Climatology of Cloud-Top Phase over the Southern Ocean and North Pacific. *J. Clim., 24* (9), 2405–18.

Morrison, A.E., Siems, S.T., Manton, M.J., and Nazarov, A. 2009. On the Analysis of a Cloud Seeding Dataset over Tasmania. *J. Appl. Meteorol. Climatol., 48,* 1267–80.

NCC. 2012. *Maps of Average Conditions* (http://www.bom.gov.au/climate/averages/maps.shtml). Australian Bureau of Meteorology, National Climate Centre, viewed August 2012.

Nicholls, N. 2010. Local and remote causes of the southern Australian autumn–winter rainfall decline, 1958–2007. *Clim. Dyn., 34* (6), 835–45.

NMOC. 2010. Operational Implementation of the ACCESS Numerical Weather Prediction systems. NMOC Operations Bulletin 83, Australian Bureau of Meteorology, National Meteorological and Oceanographic Centre.

Otkin, J.A. and Greenwald, T.J. 2008. Comparison of WRF Model-Simulated and MODIS-Derived Cloud Data. *Mon. Weather Rev., 136,* 1957–70.

Platnick, S., King, M., Ackerman, S., Menzel, W., Baum, B., Riedi, J., and Frey, R. 2003. The MODIS cloud products: Algorithms and examples from Terra. *IEEE Transactions on Geoscience and Remote Sensing, 41* (2), 459–73.

Ryan, B.F. and King, W.D. 1997. A Critical Review of the Australian Experience in Cloud Seeding. *Bull. Am. Meteorol. Soc., 78,* 239–9.

Sinclair, M.R., Wratt, D.S., Henderson, R.D., and Gray, W.R. 1997. Factors Affecting the Distribution and Spillover of Precipitation in the Southern Alps of New Zealand—A Case Study. *J. Appl. Meteorol., 36,* 428–42.

Skamarock, W.C., Klemp, J.B., Dudhia, J., Gill, D.O., Barker, D.M., Duda, M.G., Wang, W., and Powers, J.G. 2007. A Description of the Advanced Research WRF Version 2. Tech. Rep., The National Centre for Atmospheric Research.

Stephens, G.L. 1978. Radiation Profiles in Extended Water Clouds. II: Parameterization Schemes. *J. Atmos. Sci., 35*, 2123–32.

Stoelinga, M., et al. 2003. Improvement of Microphysical Parameterizations through Observational Verification Experiments (IMPROVE). *Bull. Am. Meteorol. Soc., 84*, 1807–26.

Thompson, G., Rasmussen, R.M., and Manning, K. 2004. Explicit Forecasts of Winter Precipitation Using an Improved Bulk Microphysics Scheme. Part I: Description and Sensitivity Analysis. *Mon. Weather Rev., 132* (2), 519–42.

Warburton, J.A. and Wetzel, M.A. 1992. Field study of the potential for winter precipitation enhancement in the Australian Snowy Mountains. *Atmos. Res., 28* (3–4), 327–63.

Westwater, E. 1978. The accuracy of water vapor and cloud liquid determination by dual- frequency ground-based microwave radiometry. *Radio Science, 13,* 688–685.

WMO. 2001. *WMO Executive Council—Fifty-third session (EC-LIII): abridged final report with resolutions,* 94–98. World Meteorological Association, Annex III: WMO statement on the status of weather modification.